Direct observation of shock-induced disordering of enstatite below the melting temperature

J.-A Hernandez, G. Morard, M. Guarguaglini, R. Alonso-mori, A. Benuzzi-mounaix, R. Bolis, G. Fiquet, E. Galtier, A. E Gleason, S. Glenzer, et al.

Direct observation of shock-induced disordering of enstatite below the melting temperature

J.-A. Hernandez[1,2], G. Morard[3,4], M. Guarguaglini[1], R. Alonso-Mori[5], A. Benuzzi-Mounaix[1], R. Bolis[1], G. Fiquet[3], E. Galtier[5], A. E. Gleason[5], S. Glenzer[5], F. Guyot[3], B. Ko[7], H. J. Lee[5], W. L. Mao[6], B. Nagler[5], N. Ozaki[8,9], A. K. Schuster[10,11], S. H. Shim[7], T. Vinci[1], and A. Ravasio[1]

[1]LULI, CNRS, CEA, Sorbonne Université, École Polytechnique, Institut Polytechnique de Paris, F-91128 Palaiseau, France

[2]Centre for Earth Evolution and Dynamics, University of Oslo, Norway

[3]Sorbonne Université, Institut de Minéralogie, de Physique des Matériaux et de Cosmochimie, IMPMC, UMR CNRS 7590, Museum National d'Histoire Naturelle, IRD, 4 Place Jussieu, 75005 Paris, France

[4]Institut des Sciences de la Terre, Université Grenoble-Alpes, 1381 rue de la Piscine, 38610 Gières, France

[5]SLAC National Accelerator Laboratory, 2575 Sand Hill Rd., Menlo Park, CA 94025, USA

[6]Stanford Institute for Materials and Energy Sciences, SLAC National Accelerator Laboratory, 2575 Sand Hill Rd., Menlo Park, CA 94025, USA

[7]School of Earth and Space Exploration, Arizona State University, Tempe, Arizona, USA

[8]Graduate School of Engineering, Osaka University, Suita, Osaka 565-0871, Japan

[9]Institute of Laser Engineering, Osaka University, Suita, Osaka 5650871, Japan

[10]Helmholtz-Zentrum Dresden-Rossendorf, Bautzner Landstr. 400, D-01328 Dresden, Germany

[11]Institute of Solid State and Materials Physics, Technische Universität Dresden, 01069 Dresden, Germany

Corresponding author: Jean-Alexis Hernandez (j.a.r.hernandez@geo.uio.no)

Key Points:

- We performed ultrafast X-ray diffraction of orthoenstatite crystals shock compressed up to 337±55 GPa on the Hugoniot.
- A disordered structure was observed from 80±13 GPa along the Hugoniot, well below the melting temperature.
- The degree of polymerization strongly influences the kinetics of recrystallization in shocked silicates.

Abstract

We report *in situ* structural measurements of shock-compressed single crystal orthoenstatite up to 337±55 GPa on the Hugoniot, obtained by coupling ultrafast X-ray diffraction (XRD) to laser-driven shock-compression. Shock compression induces a disordering of the crystalline structure evidenced by the appearance of a diffuse XRD signal at nanosecond time scales at 80±13 GPa on the Hugoniot, well below the equilibrium melting pressure (> 170 GPa). The formation of bridgmanite and post-perovskite have been indirectly reported in microsecond-scale plate-impact experiments. Therefore, we interpret the high-pressure disordered state we observed at nanosecond-scale as an intermediate structure from which bridgmanite and post-perovskite crystallize at longer timescales. This evidence of a disordered structure of $MgSiO_3$ on the Hugoniot indicates that the degree of polymerization of silicates is a key parameter to constrain the actual thermodynamics of shocks in natural environments.

Plain language summary

The study of silicate materials at extreme pressures and temperatures provides insight on the evolution of planetary bodies evolution during Solar System formation. During their accretion, rocky bodies have undergone several collisions and possibly planetary impacts that have transformed their minerals. The microscopic processes occurring during such events are not fully understood. In this study, we used high-power lasers to generate shock-waves into $MgSiO_3$ enstatite crystals, creating conditions comparable to the deepest part of the early Earth mantle and large planetary impacts. During the shock-wave transit, within few nanoseconds, we probed the structure of shocked enstatite between 14±3 GPa and 337±55 GPa using intense X-ray pulses from LCLS X-ray free electron laser facility. We found that, when shocked between 80±13 GPa and the conditions of equilibrium melting (above 170 GPa), enstatite transforms into a disordered structure instead of forming bridgmanite or post-perovskite – the expected equilibrium phases. This disordered structure is similar to $MgSiO_3$ glass or liquid and is observed up to 337±55 GPa. This study provides the first direct measurement of shocked enstatite structure and suggests that the observed disordered state is an intermediate phase on the transformation pathway of bridgmanite in natural impacts.

1 Introduction

The abundance of $(Mg,Fe)SiO_3$ compounds in planetary mantles and the geochemical similarities between the Earth, enstatite-rich chondrites (Dauphas 2017, Boyet et al. 2018) and/or carbonaceous chondrites (Drake and Righter 2002) requires an understanding of how space-related processes affect these meteorites before falling on Earth. In addition to space weathering and/or hydrous alteration, most meteorites have undergone multiple collisions and present evidence of shock metamorphism. These minerals can possess specific textures (e.g. mosaicism), amorphous material (e.g. formation of maskeleynite in shocked plagioclase feldspar, Jaret et al. 2015) and high-pressure polymorphs (e.g. $(Mg,Fe)_2SiO_4$ ringwoodite; $MgSiO_3$ akimotoite, majorite and bridgmanite, Binns et al., 1969, Putnis and Price 1979, Sharp et al. 1997, Zhang et al. 2006, Tschauner et al. 2014).

Structural analysis of shock-compressed enstatite recovered from gas-gun or detonation experiments (Hörz and Quaide 1973, Kozlov and Sazonova 2012) compared to minerals found in natural impacts has established impact condition indicators in enstatite chondrites (Rubin et al. 1997, Izawa et al. 2011). However, during the shock wave transit, these samples have undergone both dynamic compression up to a peak pressure and the subsequent release phase. Both loading and unloading paths induce different transformation mechanisms and their deconvolution is critical to constrain the impact history. Together with sample recovery, the acquisition of *in situ* structural data is required to identify the relevant microscopic mechanisms occurring during the different stages of the shock and their kinetics. This approach has long been prevented by technical limitations due to the short time-scales involved in laser (nanosecond) and gas-gun (microsecond) experiments.

Multiple attempts to infer the structure of shocked $MgSiO_3$ have been pursued by comparing equation of state measurements (pressure, density and temperature above 4000 K) and optical properties (Ahrens et al. 1971, Watt et al. 1986, Akins et al. 2004, Luo et al. 2004, Mosenfelder et al. 2009, Frantanduano et al. 2018) with predicted $MgSiO_3$ Hugoniot paths from atomistic simulations based on the equilibrium phase diagram (Akins et al. 2004, Militzer 2013, Soubiran et al. 2018). However, this approach is limited by the accuracy on density measurements currently achievable in shock experiments. Moreover, atomistic simulations are generally based

on equilibrium phase diagrams, while it is not well established if such equilibrium is effectively achieved at the time-scales of these experiments.

In this context, the recent coupling of ultrafast (fs) *in situ* XRD and shock compression allows direct investigation of transition mechanisms at short-time scales relevant to both gas-gun (few hundred of ns) and laser-driven (few ns) experiments. These new experimental opportunities have led to outstanding discoveries with major impacts on our understanding of shock metamorphism. Notable findings include the evidence of nanosecond scale formation of polycrystalline stishovite in shocked SiO_2 glass (Gleason et al. 2015, Tracy et al. 2018). Unfortunately, to date very few data have been reported for more complex silicates (Newman et al. 2018), and in particular for enstatite, with a higher relevance for natural environnements found in shocked meteorites.

We report direct structural measurements of laser-shocked $MgSiO_3$ enstatite between 14±3 GPa and 337±55 GPa from ultrafast *in situ* XRD.

2 Materials and Methods

The experiment was performed at the Matter in Extreme Conditions (MEC) end-station of the Linac Coherent Light Source (LCLS, Stanford, USA) by combining ultrafast XRD from the X-ray free electron laser (XFEL) at 9 keV and laser-driven shock-compression (Figure S1) of single crystals of enstatite along the [100] direction. We recorded two-dimensional XRD images in transmission geometry on four Cornell-SLAC Pixel Array Detectors (CSPADs). We determined the uniaxial pressure by measuring fluid and/or mean shock velocities using a velocity interferometer system for any reflector (VISAR) and existing refractive index and equation of state measurements of shocked enstatite on the principal Hugoniot (Luo et al. 2004, Akins et al. 2004, Mosenfelder et al. 2009, Fratanduono et al. 2018). By varying the drive laser energies and by adjusting the delay between the drive lasers and the 60 fs (pulse width) XFEL pulse, we captured quasi-instantaneous snapshots of the structure of uniformly shocked enstatite between 14±3 GPa and 337±55 GPa.

2.1 Target preparation

Planar multilayered targets (Figure S1b) were composed of a 50 μm-thick polystyrene (PS) ablator glued to the enstatite sample. We first coated both the ablator and the sample with 300 nm Ti on the drive laser side prior gluing. The Ti coating on the ablator prevented the drive laser from shining through it. On the sample, it acts as a reflective layer for optical diagnostics. Natural orthoenstatite single crystals of gem quality (loc. Mogok, Myanmar) were first cut into 2×2 mm plates perpendicular to the [100] direction and polished down to a thickness of 50-60 μm. Two groups of orthoenstatite crystals were used with initial densities of 3.219 and 3.259 $g.cm^{-3}$ (respective compositions of $Mg_{0.98}Fe_{0.02}SiO_3$ and $Mg_{0.93}Fe_{0.07}SiO_3$). Using confocal imagery and interferometry we measured the thickness and the planarity of each sample with accuracy <100 nm and selected only those thinner than 57±1 μm. We optimized the PS and enstatite thicknesses for shock stationarity in concert with hydrodynamic simulations made with the Lagragian one-dimensional code MULTI (Ramis et al. 1988). We designed additional targets with a LiF window behind the sample (see section S1) to verify that steady conditions are maintained during the shock transit through the sample.

2.2 Laser-driven dynamic compression

Uniaxial dynamic compression was achieved by launching a shock wave using two frequency-doubled Nd-glass MEC laser beams with 10 ns square pulses operating at 527 nm (Figure S1a). The flatness and uniformity of the 250 μm-diameter focal spot was achieved by using continuous phase plates. In this configuration we obtained a maximum intensity on target of $I_L \sim 10^{13}$ $W.cm^{-2}$. In order to reach higher intensities, required to melt enstatite, we removed the phase plates and focused the two laser beams into smaller Gaussian spot profiles. In this case, we carefully checked the shock planarity and the overlap between the drive laser and the X-ray beam focal spots.

Characteristic velocities of shock-compressed enstatite were measured using VISAR with a probe laser operating at a wavelength of 532 nm. Space-time images were recorded on an ultrafast streak camera with ~100 ps time resolution. The velocity changes of the reflecting interface(s) were detected from interference fringe shifts. VISAR channel sensitivities were 4.658 $km.s^{-1}.fringe^{-1}$ and 1.814 $km.s^{-1}.fringe^{-1}$. Shock-compressed enstatite remains transparent on the principal Hugoniot at least up to 164 GPa (Fratanduono et al. 2018). In this pressure range we measured the velocity of the Ti/enstatite interface (by reflecting off the thin Ti coating),

which corresponds to the apparent fluid velocity of the shocked enstatite. We deduced the true fluid velocity (U_p) by correcting the apparent velocity for the change of refractive index in the shocked enstatite according to the linear dependence on density given in Fratanduono et al. (2018). The shock breakout also induces a fringe shift due to the large change of refractive index between the vacuum and the shock front on the rear side of the target. The delay between the shock entrance in the enstatite and the shock breakout determines the mean shock velocity (U_s). For high intensity shots, the shocked enstatite became opaque and the thermodynamic conditions were deduced from the measured mean shock velocity U_s and the Hugoniot relation of Fratanduono et al. (2018). Pressure and density are then determined from U_s and U_p via Rankine-Hugoniot relations.

2.4 Ultrafast X-ray diffraction

In situ XRD was performed using quasi-monochromatic (dE/E = 0.2-0.5 %) 9 keV X-ray pulses of 60 fs duration with an average intensity of ~10^{12} photons per pulse. The XFEL beam had a normal incidence on the target surface and a 20° angle with the drive laser arms. LCLS XFEL spot diameter was set to 50 μm, which is much smaller than the flat-compressed region so as to avoid probing regions affected by pressure and temperature gradients. As X-rays probe the bulk sample, special attention was paid to ensure uniform thermodynamic conditions in the shocked part, both by optimizing target design and probing times. Two-dimensional XRD images were recorded in transmission geometry on the four CSPADs. CSPADs were calibrated with powders of CeO_2 674a and LaB_6 660a NIST standard reference materials. For each target, a reference XRD pattern of the unshocked sample was acquired prior to shock compression. Additional details about the azimuthal integration procedure are given in Section S3.

3 Results

3.1 *In situ* X-ray diffraction of shock-compressed orthoenstatite

Figure 1 shows the evolution of the XRD patterns obtained at different pressures along the principal Hugoniot of enstatite 1.7-6 ns after the shock entrance in the sample and before the shock breakout. Between 14±3 GPa and 79±26 GPa, i.e. above the Hugoniot elastic limit of enstatite and within the so-called mixed phase region (MPR, Akins et al. 2004), only single

crystal patterns attributed to pyroxenoid (i.e. pyroxene-like) structures, are recorded at nanosecond time-scale during the shock (e.g. Figure 1, 14±3 GPa and 76±17 GPa). The different single crystal XRD patterns were tentatively attributed to metastable structures described by Finkelstein et al. (2015) such as compressed enstatite and β-post-orthopyroxene (β-popx, see section S4).

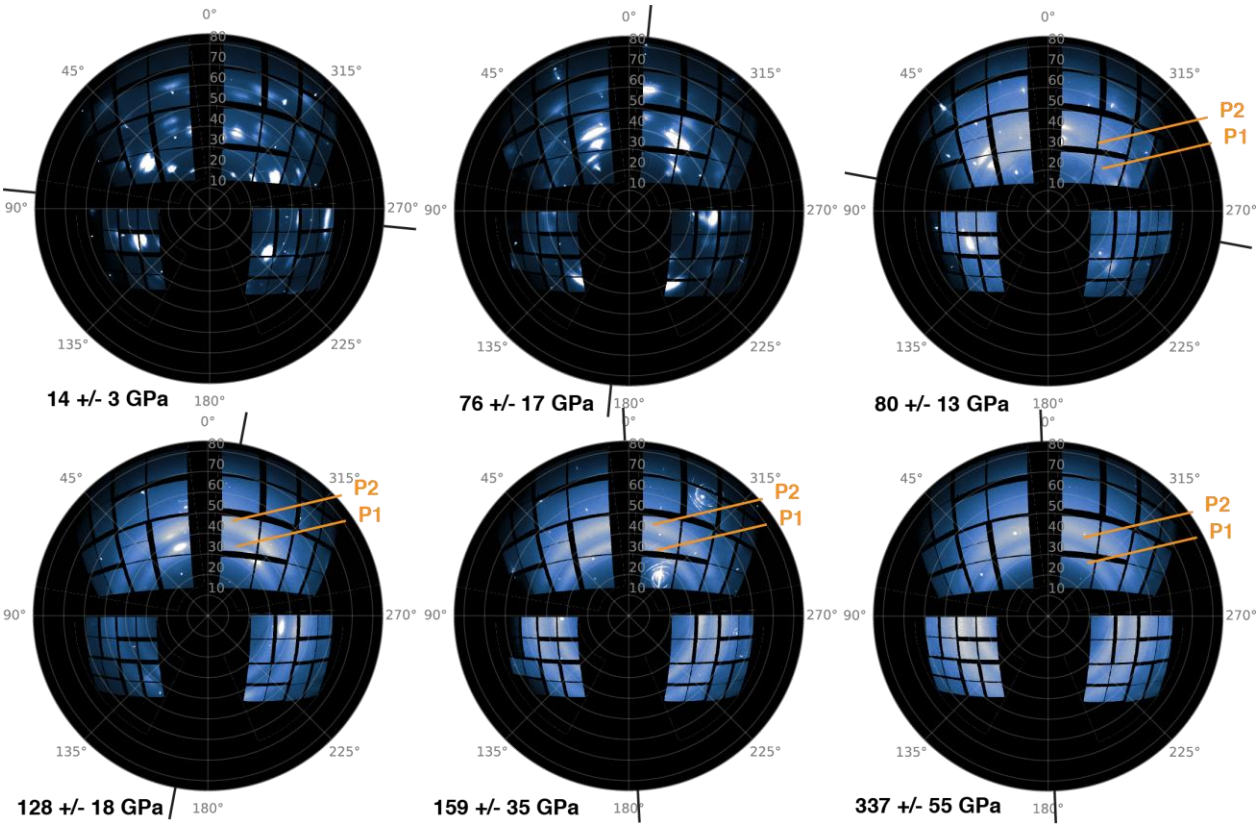

Figure 1: Experimental *in situ* XRD data recorded at peak pressure in laser-shocked single crystal enstatite oriented along [100]. Images from the four CSPAD are projected in the (2θ, ϕ) coordinate system. Black ticks indicate sample relative rotations along the shock and XFEL axis. The intense few pixel-wide diffraction spots present on all images come from the unshocked part of the enstatite sample; wide spots with variable intensities visible up to 128±18 GPa originate from the shocked sample and can be reproduced considering two pyroxenoids (Figure S4). Enstatite transformation toward a disordered structure begins at 80±13 GPa, well below melting conditions, with the appearance of two diffuse rings, labelled P1 and P2. Above 128±18 GPa, the diffraction spots of dense pyroxenoid structures disappear and only features P1 and P2 remain. At 337±55 GPa, enstatite is shocked in the liquid state.

Between 80±13 GPa and 128±18 GPa, pyroxenoid structures persist and coexist with two diffuse rings at 2θ~35° and 2θ~44°, respectively denoted P1 and P2, whose intensities increase with

pressure. For all shocks above 129±20 GPa, only the diffuse rings come from the shocked enstatite (see shocks at 159±35 and 337±55 GPa in Figure 1).

Azimuthal integration of the diffuse signal was done as a function of pressure and density along the Hugoniot (Figure 2). We first investigate the possibility that the diffuse pattern is produced by bridgmanite (Bd) or post-perovskite (Ppv), the thermodynamically stable phases between 80±13 GPa and the equilibrium melting line (i.e. above 170 GPa). The comparison of our spectra with simulated diffraction patterns (Figure S5) of both polycrystalline Bd and Ppv with 3 nm-large crystals (twice smaller than first stishovite crystals observed in laser-shocked silica glass, Gleason et al. 2015) excludes the formation of these high-pressure polymorphs at nanosecond scale. Then, the spectra and the positions of P1 and P2 were compared, and found to be similar to the ones obtained in both static and dynamic compression experiments performed on $MgSiO_3$ glass (Kono et al, 2018, Morard et al. 2020). Fourier transform analyses of these compressed glasses have shown that both the appearance of P2, and the shift toward higher q-values of P1, are attributed to the continuous change from 4-fold to 6-fold Si-O coordination (Ghosh et al. 2014, Kono et al. 2018). By analogy, we suggest that enstatite transforms into a disordered phase under shock-compression at nanosecond-scale between 80±13 GPa and 179±37 GPa, which changes continuously toward a six-fold Si-O structure. Complete refinement at the atomic scale would require larger q-range. Based on our previous measurements on $MgSiO_3$ glass (Morard et al. 2020) we find a striking agreement for peak positions of diffuse signal from cold compressed glass and shocked disordered enstatite at similar densities (Figure 2), suggesting the transformation of crystalline enstatite into a six-fold Si-O disordered structure under shock compression.

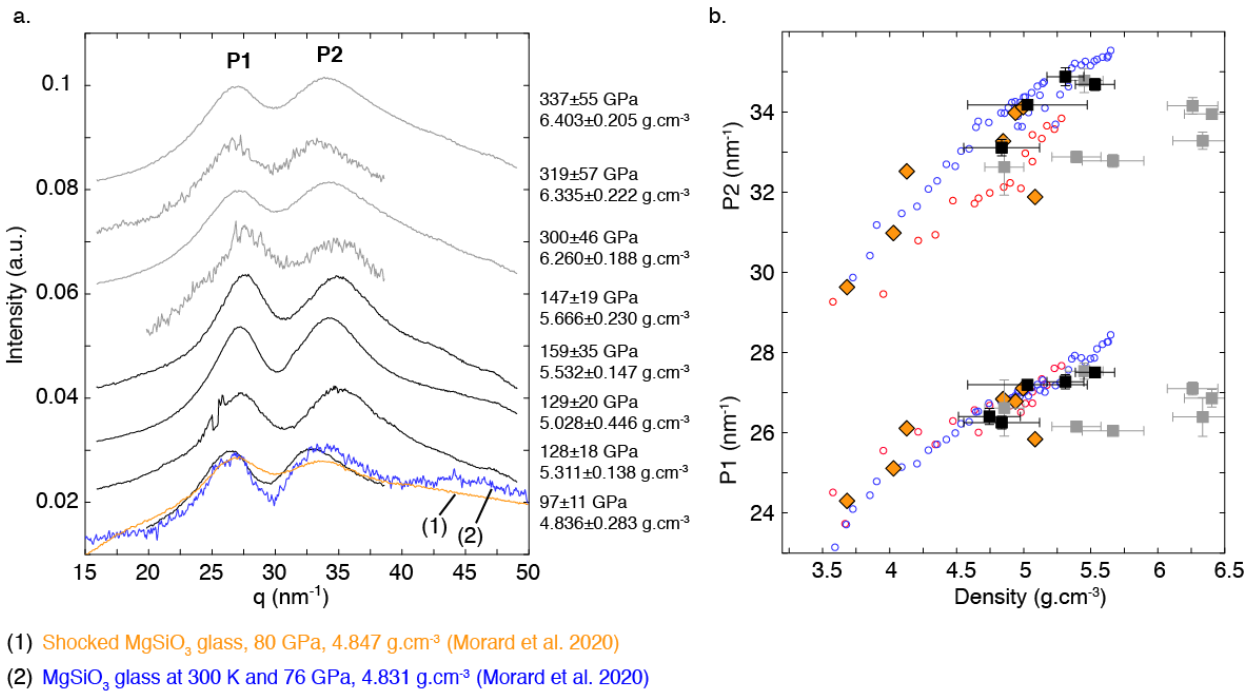

Figure 2: a. Azimuthal integration of the disordered component observed in shocked orthoenstatite between 97±11 GPa and 337±55 GPa (black and grey lines respectively indicate shots with and without phase plate). Diffraction spots coming either from the unshocked part of the target or from dense pyroxenoids have been masked before the integration. The norm of the scattering vector q is related to the Bragg angle by $q = 4\pi \sin(\theta) / \lambda$. All spectra are normalized with respect to their area. The spectrum at 97±11 GPa is compared to two spectra obtained from statically compressed $MgSiO_3$ glass at 300 K (blue) and from laser-shocked $MgSiO_3$ glass (orange) at comparable density (Morard et al. 2020). Our data show that all three spectra are similar and demonstrate the typical of 6-fold Si-O coordinated features in silicates with P2 arising under compression above several GPa (Sanloup et al. 2013, Ghosh et al. 2014, Zeidler and Salmon 2016, Prescher et al. 2017, Kono et al. 2018, Morard et al. 2020). **b.** Positions of P1 and P2 as function of density. Squares represent the data obtained in the present shock experiment, where the density is determined from VISAR measurements. Empty circles correspond to statically compressed $MgSiO_3$ at 300 K (red: from Kono et al. 2018, blue: from Morard et al. 2020). Corresponding densities have been derived from pressures based on the equation of state of Petitgirard et al. (2015). Orange diamonds refer to shocked $MgSiO_3$ glass (Morard et al. 2020).

The presence of diffuse rings on the XRD patterns does not allow us to discriminate between a hot metastable amorphous or a liquid phase. Consensus on the exact melting pressure on the shock Hugoniot does not exist, however, all theoretical and experimental studies place it above 170-180 GPa (Akins et al. 2004, Belonoshko et al. 2005, Stixrude et al. 2005, De Koker et al. 2009, Mosenfelder et al. 2009). Recent laser experiments suggest a complete melting pressure as high as 227±10 GPa from a slope change in the thermal emission of the sample in a decaying

shock experiment (Fratanduono et al. 2018). In addition, VISAR images show that at 128±18 GPa and 159±35 GPa, shocked $MgSiO_3$ presents a large absorption length of ~20 μm at 532 nm, in good agreement with Fratanduono et al. (2018) at sub-melting conditions (see Figure S6). On the contrary, the VISAR data for the experiment above 300±46 GPa (Figure S6) only show only ghost fringes due to an interfering reflection on the rear side of the silicate (no anti-reflection coating), indicating that $MgSiO_3$ is opaque or weakly reflecting. This is consistent with the properties predicted for the equilibrium liquid in Soubiran et al. (2018).

Figure 3.a shows the pressures and densities of shocked enstatite deduced from our velocity measurements with the corresponding lattice structure probed by XRD at nanosecond timescales. Figure 3.b shows existing pressure-density measurements obtained in gas-gun experiments at the microsecond scale and the interpreted phases from velocimetry. The pressure range in which we observe crystalline XRD patterns corresponds to three different regimes on the microsecond scale Hugoniot: compressed enstatite up to 15 GPa; a mixed phase region that is expected to contain multiple phases (Akins et al. 2004) and extend up to 70 GPa; akimotoite (70-90 GPa). The disordering of enstatite observed in our experiment occurs at conditions where Bd and Ppv are considered to form at microsecond scale, and leads us to consider disordered $MgSiO_3$ as a reaction intermediate in the formation of Bd and Ppv from shocked enstatite.

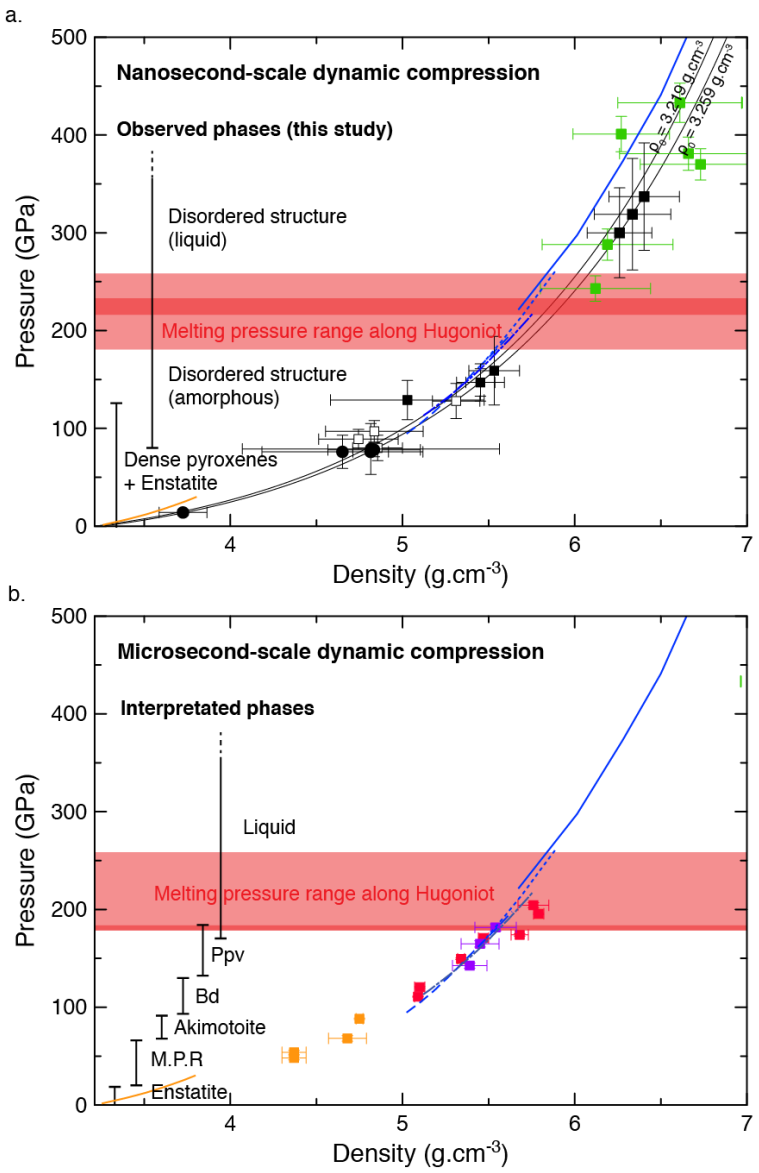

Figure 3: Pressure-density diagrams of shock-compressed enstatite at nanosecond-scale (a.) and microsecond-scale (b.). a. We distinguish the shots in which only compressed enstatite and a dense pyroxene-like structure have been observed (black dots) from those in which they coexist with disordered $MgSiO_3$ (white squares). Filled squares correspond to the shots where the signal of the disordered structure only comes from the shocked part of the target. Green squares represent measurements from Frantanduono et al. (2018). b. Squares correspond to data from gas-gun experiments: orange, Akins et al. (2004); red, Akins et al. (2004) data reanalyzed by Mosenfelder et al. (2009); purple; Luo et al. (2004) data reanalyzed by Mosenfelder et al. (2009). The black line corresponds to the linear fit of all shock versus fluid velocity as done in Fratanduono et al. (2018). Blue curves represent calculated Hugoniot paths from atomistic simulations at thermodynamic equilibrium based on density functional theory (continuous, liquid from Militzer 2013; dotted, Ppv from Militzer 2013; dash-dotted, glass from Wolf et al. 2019 based on data from DeKoker and Stixrude 2009; dashed, Bd from Akins et al. 2004). The orange line is the Hugoniot of enstatite (Akins 2003). In panel a., the dark red area corresponds to the melting pressure of shocked enstatite (227±10 GPa)

estimated from laser decaying shock experiments from Frantanduono et al. (2018). In panel b., it represents the melting pressure estimated from gas-gun experiments in Mosenfelder et al. (2009). The pale red area indicates the melting pressure range along the enstatite Hugoniot considering DFT-MD simulations from Militzer et al. (2013).

4 Discussion

In order to understand transformation kinetics in shocked enstatite and to overcome the limitations inherent to the pressure-density diagram, we investigate possible temperature differences between $MgSiO_3$ enstatite shocked state formed in gas gun (microsecond equilibration at peak pressure) and in laser experiments (nanosecond equilibration at peak pressure). The following interpretation is based on an analogy with recent results on shocked SiO_2 (Shen et al. 2016a, 2016b, Gleason et al. 2015, Gleason et al. 2017) and assumes that Bd or Ppv actually form in gas gun experiments as interpreted in Akins et al. (2003), Luo et al. (2004) and Mosenfelder et al. (2009).

In shocked SiO_2, polycrystalline stishovite nucleates and grows within few nanoseconds from a 6-fold Si-O coordinated amorphous phase that has the same structure as the melt obtained at higher pressures (Shen et al. 2016a, 2016b; Gleason et al. 2015). Hundred picoseconds behind the shock front, the thermodynamic conditions in the high-pressure amorphous state lay on the extension of the liquid state Hugoniot below the equilibrium melting line (Figure S7). During crystallization, temperature increases by ~1000 K up to the Hugoniot of stishovite (Shen et al. 2016a, 2016b) although pressure and density do not change significantly compared to the reachable experimental accuracy. We propose that such mechanism occurs in shocked $MgSiO_3$ but at longer time scales.

Since optical emission of shocked enstatite was not recorded in our experiment, we estimated the temperature of our shots – in which disordered $MgSiO_3$ has formed – based on existing Hugoniot measurements of liquid $MgSiO_3$ (Fratanduono et al. 2018) and Hugoniot predictions for both liquid and glassy $MgSiO_3$ from atomistic simulations (DeKoker and Stixrude 2009, Militzer 2013 and Millot et al. 2020), which all use an initial density of 3.22-3.26 $g.cm^{-3}$ (Figure 4). The resulting temperatures at 80±13 GPa and at 159±35 GPa differ by 500-1500 K with existing gas gun measurements (Luo et al. 2004), and *a contrario*, are in an excellent agreement with the Hugoniot of Ppv deduced from equilibrium atomistic simulations (Militzer et al. 2013). This difference between the shock temperature estimated in our ns-scale experiment (with *in situ*

observation of disordered $MgSiO_3$) and the shock temperature measured in µs-scale experiments (which compressed state is interpretated as Bd or Ppv based on compression curves) suggests that shocked orthoenstatite first amorphizes and recrystallizes into Bd or Ppv within few microseconds. Therefore, the crystallization kinetics of high-pressure polymorphs in shocked $MgSiO_3$ would be 2-3 orders of magnitude slower than the one occurring in SiO_2. This reveals that the degree of polymerization of shocked silicates may be a key parameter to understand recrystallization kinetics in natural environment, e.g. shock veins in meteorites for example.

We mention that the crystalline state of the unshocked sample does not influence the kinetics of crystallization since we observed the same behavior when starting from $MgSiO_3$ glass (Morard et al. 2020).

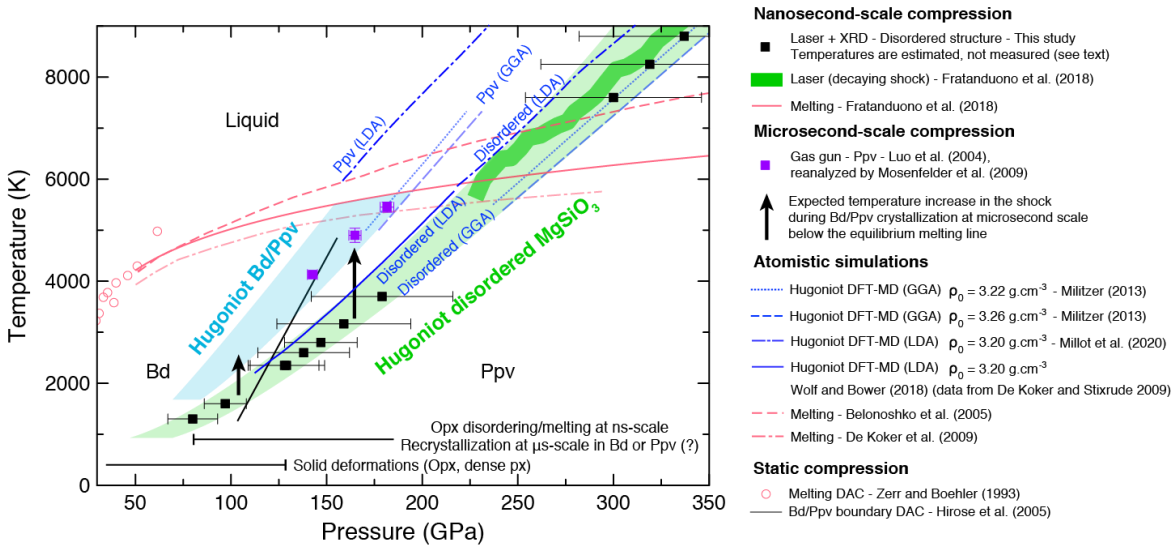

Figure 4: Phase diagram of $MgSiO_3$. Hugoniot measurements are all performed from shock-compressed enstatite. Assuming that $MgSiO_3$ behaves similarly as SiO_2 when shocked, i.e. high-pressure polymorphs crystallize from a high-pressure amorphous metastable phase similar to the equilibrium melt, we estimate the temperature of the amorphous and melt samples (probed in this study by *in situ* XRD) based on the extrapolation of the melt Hugoniot measured by decaying shock at nanosecond timesscales (Fratanduono et al. 2018). The resulting temperature difference between the amorphous material formed after a few ns and the gas-gun microsecond timescale measurements may indicate the crystallization of $MgSiO_3$ bridgmanite or post-perovskite at microsecond timescales. As such, the equilibrium Hugoniot (as calculated from DFT assuming a Ppv structure) would be reached after a few microseconds.

5 Conclusions

We studied the structure of shocked [100] orthoenstatite using ultrafast XRD. We found that orthoenstatite densifies while keeping crystalline pyroxene-like structures up to 76±17 GPa. At 80±13 GPa and above, it amorphizes into a dense disordered phase with the same structure as observed in statically compressed $MgSiO_3$ glass. Between 80±13 GPa and 128±18 GPa, the signal of the disordered phase coexists with diffraction spots from pyroxene-like structures, indicating that disordering is incomplete or occurs after first crystalline transformations. Between 128±18 GPa and the melting conditions, only the disordered phase is observed. The liquid, sampled between 300±46 GPa and 337±55 GPa, presents a similar structure. We propose that the disordered state is a reaction intermediate on the transition pathway towards dense $MgSiO_3$ polymorphs, such as akimotoite, bridgmanite and post-perovskite, that would crystallize from it at peak pressure. As these high-pressure polymorphs have been indirectly shown to form in microsecond scale shock experiments (Akins et al. 2004, Luo et al. 2004, Mosenfelder et al. 2009), and are absent from our nanosecond scale measurements, we expect their crystallization to occurs within 0.01-1 μs. This differs significantly from the crystallization kinetics of stishovite in shocked SiO_2 which occurs at (sub-)nanosecond scale (Gleason et al. 2015, Shen et al. 2016a). Future XRD measurements should investigate the formation of Bd and Ppv at microsecond scale in shock-compressed enstatite, i.e. using a gas gun facility.

Acknowledgments and Data Avalaibility

The authors thank Y. Kono for sharing his dataset and F. Lefevre, N. Coudurier, M. A. Baron, B. Baptiste for helping with the target fabrication and characterization. This research was supported by the POMPEI program of the Agence National de la Recherche (Grant ANR-16-CE31-0008). G.M., G.F. and F.G. acknowledge funding from the European Research Council (ERC) under the EU-H2020 research and innovation program (ERC PLANETDIVE grant agreement 670787). A. E. G. acknowledges the LANL Reines LDRD. A. E. G. and W. M. acknowledge support from the NSF Geophysics Program (EAR0738873). A.K.S. is supported by the Helmholtz Association under VH-NG-1141. The experiment was performed at the MEC instrument of LCLS, supported by the U.S. DOE Office of Science, Fusion Energy Science under contract No. SF00515, FWP 100182, and by LCLS, a National User Facility operated by Stanford University on behalf of the

U.S. DOE, Office of Basic Energy Sciences. N. O. acknowledges support from JSPS core-to-core program on International Alliance for Material Science in Extreme States with High Power Laser and XFEL and MEXT XFEL Priority Strategy Program at Osaka University (contract 12005014). Data can be found online at osf.io/jz9wt.

References

Ahrens, T. J., & Gaffney, E. S. (1971). Dynamic compression of enstatite. *Journal of Geophysical Research*, *76*(23), 5504-5513.

Akins, J. A. (2003). *Dynamic compression of minerals in the MgO-FeO-SiO2 system* (Doctoral dissertation, California Institute of Technology).

Akins, J. A., Luo, S. N., Asimow, P. D., & Ahrens, T. J. (2004). Shock-induced melting of MgSiO3 perovskite and implications for melts in Earth's lowermost mantle. *Geophysical Research Letters*, *31*(14).

Ashiotis, G., Deschildre, A., Nawaz, Z., Wright, J. P., Karkoulis, D., Picca, F. E., & Kieffer, J. (2015). The fast azimuthal integration Python library: pyFAI. *Journal of applied crystallography*, *48*(2), 510-519.

Belonoshko, A. B., Skorodumova, N. V., Rosengren, A., Ahuja, R., Johansson, B., Burakovsky, L., & Preston, D. L. (2005). High-pressure melting of MgSiO 3. *Physical review letters*, *94*(19), 195701.

Binns, R. A., Davis, R. J., & Reed, S. J. B. (1969). Ringwoodite, natural (Mg, Fe)2SiO4 spinel in the Tenham meteorite. *Nature*, *221*(5184), 943-944.

Boyet, M., Bouvier, A., Frossard, P., Hammouda, T., Garçon, M., & Gannoun, A. (2018). Enstatite chondrites EL3 as building blocks for the Earth: The debate over the 146Sm–142Nd systematics. *Earth and Planetary Science Letters*, *488*, 68-78.

Dauphas, N. (2017). The isotopic nature of the Earth's accreting material through time. *Nature*, *541*(7638), 521-524.

Drake, M. J., & Righter, K. (2002). Determining the composition of the Earth. *Nature*, *416*(6876), 39-44.

De Koker, N., & Stixrude, L. (2009). Self-consistent thermodynamic description of silicate liquids, with application to shock melting of MgO periclase and MgSiO3 perovskite. *Geophysical Journal International*, *178*(1), 162-179.

Finkelstein, G. J., Dera, P. K., & Duffy, T. S. (2015). Phase transitions in orthopyroxene (En90) to 49 GPa from single-crystal X-ray diffraction. *Physics of the Earth and Planetary Interiors*, *244*, 78-86.

Fratanduono, D. E., Millot, M., Kraus, R. G., Spaulding, D. K., Collins, G. W., Celliers, P. M., & Eggert, J. H. (2018). Thermodynamic properties of MgSiO 3 at super-Earth mantle conditions. *Physical Review B*, *97*(21), 214105.

Ghosh, D. B., Karki, B. B., & Stixrude, L. (2014). First-principles molecular dynamics simulations of MgSiO3 glass: Structure, density, and elasticity at high pressure. *American Mineralogist*, *99*(7), 1304-1314.

Gleason, A. E., Bolme, C. A., Lee, H. J., Nagler, B., Galtier, E., Milathianaki, D., ... & Collins, G. W. (2015). Ultrafast visualization of crystallization and grain growth in shock-compressed SiO2. *Nature communications*, *6*(1), 1-7.

Gleason, A. E., Bolme, C. A., Lee, H. J., Nagler, B., Galtier, E., Kraus, R. G., ... & Mao, W. L. (2017). Time-resolved diffraction of shock-released SiO 2 and diaplectic glass formation. *Nature communications*, *8*(1), 1-6.

Hörz, F., & Quaide, W. L. (1973). Debye-Scherrer investigations of experimentally shocked silicates. *The Moon*, *6*(1-2), 45-82.

Izawa, M. R., Flemming, R. L., Banerjee, N. R., & McCAUSLAND, P. J. (2011). Micro-X-ray diffraction assessment of shock stage in enstatite chondrites. *Meteoritics & Planetary Science*, *46*(5), 638-651.

Jaret, S. J., Woerner, W. R., Phillips, B. L., Ehm, L., Nekvasil, H., Wright, S. P., & Glotch, T. D. (2015). Maskelynite formation via solid-state transformation: Evidence of infrared and X-ray anisotropy. *Journal of Geophysical Research: Planets*, *120*(3), 570-587.

Kono, Y., Shibazaki, Y., Kenney-Benson, C., Wang, Y., & Shen, G. (2018). Pressure-induced structural change in MgSiO3 glass at pressures near the Earth's core–mantle boundary. *Proceedings of the National Academy of Sciences*, *115*(8), 1742-1747.

Kozlov, E. A., & Sazonova, L. V. (2012). Phase transformations of enstatite in spherical shock waves. *Petrology*, *20*(4), 336-346.

Luo, S. N., Akins, J. A., Ahrens, T. J., & Asimow, P. D. (2004). Shock-compressed MgSiO3 glass, enstatite, olivine, and quartz: Optical emission, temperatures, and melting. *Journal of Geophysical Research: Solid Earth*, *109*(B5).

Militzer, B. (2013). Ab initio investigation of a possible liquid–liquid phase transition in MgSiO3 at megabar pressures. *High Energy Density Physics*, *9*(1), 152-157.

Millot, M., Zhang, S., Fratanduono, D. E., Coppari, F., Hamel, S., Militzer, B., ... & Eggert, J. H. (2020). Recreating Giants Impacts in the Laboratory: Shock Compression of Bridgmanite to 14 Mbar. *Geophysical Research Letters*, *47*(4)

Morard, G., Hernandez, J. A., Guarguaglini, M., Bolis, R., Benuzzi-Mounaix, A., Vinci, T., ... & Gleason, A. E. (2020). In situ X-ray diffraction of silicate liquids and glasses under dynamic and static compression to megabar pressures. *Proceedings of the National Academy of Sciences*, *117*(22), 11981-11986.

Mosenfelder, J. L., Asimow, P. D., Frost, D. J., Rubie, D. C., & Ahrens, T. J. (2009). The MgSiO3 system at high pressure: Thermodynamic properties of perovskite, postperovskite, and melt from global inversion of shock and static compression data. *Journal of Geophysical Research: Solid Earth*, *114*(B1).

Newman, M. G., Kraus, R. G., Akin, M. C., Bernier, J. V., Dillman, A. M., Homel, M. A., ... & Sinclair, N. W. (2018). *In situ* observations of phase changes in shock compressed forsterite. *Geophysical Research Letters*, *45*(16), 8129-8135.

Petitgirard, S., Malfait, W. J., Sinmyo, R., Kupenko, I., Hennet, L., Harries, D., ... & Rubie, D. C. (2015). Fate of MgSiO3 melts at core–mantle boundary conditions. *Proceedings of the National Academy of Sciences*, *112*(46), 14186-14190.

Prescher, C., Prakapenka, V. B., Stefanski, J., Jahn, S., Skinner, L. B., & Wang, Y. (2017). Beyond sixfold coordinated Si in SiO2 glass at ultrahigh pressures. *Proceedings of the National Academy of Sciences*, *114*(38), 10041-10046.

Putnis, A., & Price, G. D. (1979). High-pressure (Mg, Fe) 2 SiO 4 phases in the Tenham chondritic meteorite. *Nature*, *280*(5719), 217-218.

Ramis, R., Schmalz, R., & Meyer-ter-Vehn, J. (1988). MULTI—A computer code for one-dimensional multigroup radiation hydrodynamics. *Computer Physics Communications*, *49*(3), 475-505.

Rubin, A. E., Scott, E. R., & Keil, K. (1997). Shock metamorphism of enstatite chondrites. *Geochimica et Cosmochimica Acta*, *61*(4), 847-858.

Sanloup, C., Drewitt, J. W. E., Crépisson, C., Kono, Y., Park, C., McCammon, C., ... & Bytchkov, A. (2013). Structure and density of molten fayalite at high pressure. *Geochimica et Cosmochimica Acta*, *118*, 118-128.

Sharp, T. G., Lingemann, C. M., Dupas, C., & Stöffler, D. (1997). Natural occurrence of MgSiO3-ilmenite and evidence for MgSiO3-perovskite in a shocked L chondrite. *Science*, *277*(5324), 352-355.

Shen, Y., Jester, S. B., Qi, T., & Reed, E. J. (2016). Nanosecond homogeneous nucleation and crystal growth in shock-compressed SiO2. *Nature materials*, *15*(1), 60-65.

Shen, Y., & Reed, E. J. (2016). Quantum nuclear effects in stishovite crystallization in shock-compressed fused silica. *The Journal of Physical Chemistry C*, *120*(31), 17759-17766.

Soubiran, F., & Militzer, B. (2018). Electrical conductivity and magnetic dynamos in magma oceans of Super-Earths. *Nature communications*, *9*(1), 1-7.

Stixrude, L., & Karki, B. (2005). Structure and freezing of MgSiO3 liquid in Earth's lower mantle. *Science*, *310*(5746), 297-299.

Tracy, S. J., Turneaure, S. J., & Duffy, T. S. (2018). *In situ* x-Ray diffraction of shock-compressed fused silica. *Physical review letters*, *120*(13), 135702.

Tschauner, O., Ma, C., Beckett, J. R., Prescher, C., Prakapenka, V. B., & Rossman, G. R. (2014). Discovery of bridgmanite, the most abundant mineral in Earth, in a shocked meteorite. *Science*, *346*(6213), 1100-1102.

Watt, J. P., & Ahrens, T. J. (1986). Shock wave equation of state of enstatite. *Journal of Geophysical Research: Solid Earth*, *91*(B7), 7495-7503.

Zeidler, A., & Salmon, P. S. (2016). Pressure-driven transformation of the ordering in amorphous network-forming materials. *Physical Review B*, *93*(21), 214204.

Zhang, A., Hsu, W., Wang, R., & Ding, M. (2006). Pyroxene polymorphs in melt veins of the heavily shocked Sixiangkou L6 chondrite. *European Journal of Mineralogy*, *18*(6), 719-726.